Design and Analysis of Computer Disk Drive Suspension Vibration Compensation Control

Xinghui Huang, Yunfeng Li and Roberto Horowitz
Computer Mechanics Laboratory (CML)
Department of Mechanical Engineering
University of California at Berkeley, CA 94720-1740
{xhhuang,yunfeng,horowitz}@me.berkeley.edu

Abstract

Based on the existing dual-stage control scheme for hard disk drives, this paper focuses on the design and analysis of adaptive feedforward control of airflow induced suspension vibration, which utilizes the vibration signal obtained from instrumented suspension. In this scheme, a strain signal on the surface of the instrumented suspension is obtained which is indicative of the suspension's vibration motion. The slider at the tip of the suspension is controller by a MEMS microactuator (MA). The effect of MA resonance mode variations on the performance of the controllers are also analyzed. Online identification of the MA model can be added to this structure to compensate for the variations in MA's resonance mode. Simulations show that the proposed technique can successfully suppress the suspension vibration induced TMR and is suited for use in increasingly high track density, high performance hard disk drives.

1 Introduction

With the technological advances and breakthroughs in computer hard disk drives (HDD), there has been a continuing trend of increasing areal storage density from 100 Mb/in^2 in 1991 toward the goal of about 100 Gb/in^2 recently. It is predicted that future areal storage density increases will be achieved mainly through an increase in track density. For a predicted bit aspect ratio of 4:1, an areal density of 100 Gb/in^2 corresponds to a linear bit density of 672k bits per inch (BPI), and a radial track density of 168k tracks per inch (TPI), or equivalently, a track pitch of 150 nm. Higher track density implies narrower track width and, consequently, smaller tracking errors. To achieve effective settling and tracking following at these higher track densities, the closed-loop bandwidth of the servo system must increase without compromising track access time. Dual-stage control structure has been proposed to satisfy this requirement and achieve better performance. It is shown that most of the TMR due to track runout and low-frequency disturbances in hard disk drives can be greatly attenuated by extending the bandwidth of the track following servo by properly designing the dual-stage controller. However, experiments also show that, with increased spindle rotation speed, airflow induced suspension vibration will become a major obstacle to achieving higher track density. This type of vibration manifests itself around the structure resonance modes of the suspension which are generally located beyond the scope of the predicted servo bandwidth. Since the servo bandwidth is limited by the sampling rate of position error signal (PES), the TMR due to suspension vibration cannot be efficiently attenuated with only PES feedback control. On the contrary, airflow induced suspension vibration may be amplified by the feedback controller due to the waterbed effect of the closed-loop sensitivity transfer function (TF)[1].

The idea of utilizing additional sensors to further increase the actuator bandwidth has been proposed and explored by several authors [2][3][4][5]. In [2][3][4], it is proposed to attach an acceleration sensor at a proper location of a hard disk drive to provide the feedforward vibration signal. All those schemes are based on a single actuator, voice coil motor (VCM). They may be referred to as single-stage plus feedforward structures. Generally, commercial VCMs have limited bandwidth of about 400-700 Hz due to the existence of E-block and suspension resonance modes. Therefore, the single-stage servo structure can only cancel out those vibration modes that are within VCM's achievable dynamics bandwidth. Higher track following precision and shorter settling time cannot be achieved without adding an auxiliary microactuator with faster dynamics. In [5], adaptive feedforward control was designed to cancel suspension vibration by using the strain signal on the surface of the instrumented suspension, and controlling slider with a MEMS microactuator. Since this is a dual-stage plus feedforward control structure, better performance is expected on the basis of the achieved performance of a normal dual-stage controller. With increasing spindle rotation speed, the airflow excitation impinging on the actuator arm is becoming a more and more important factor affecting TMR. From the experimental results of [5], airflow affects TMR mainly by exciting suspension's own resonance modes. This observation points toward the possibility of using the strain signal on the surface of the suspension for control, in order to suppress airflow induced TMR.

In this paper, an adaptive feedback plus feedforward control is proposed for airflow induced suspension vibration compensation. It is an actuated slider dual-stage servo system, which utilizes a MEMS MA positioned at the end of the suspension. For the MA control input, both feedback and feedforward gains are updated online to minimize the variance of the PES. By comparing with several other schemes through simulation, it is shown that this control scheme can effectively attenuate the airflow induced structural vibration and achieve the best track following performance.

This paper is organized as follows: Section 2 discusses the impact of airflow induced suspension vibration on the suspension op-

eration and the hardware structure of the MEMS microactuator based dual-stage servo. The detailed structure and derivation of the proposed adaptive feedback and feedforward vibration control scheme is presented in Section 3. Simulation results and analysis are shown in Section 4. Conclusions are provided in Section 5.

2 Airflow Induced Suspension Vibration and Dual-stage Servo Structure

The excitation magnitude of airflow is roughly related to the following three aspects: disk's rotation speed, the radial location of the suspension with respect to the disk, and the viscosity of air. Especially, the spindle rotation speed has a big impact on the airflow induced suspension vibration. The estimated root mean square value of TMR due to airflow is about 5.8 nm for the disk rotation speed of 10k rpm. While the TMR budget (σ value) for 100k TPI is about 8 nm. One can see that airflow induced structural vibration constitutes the main portion of TMR.

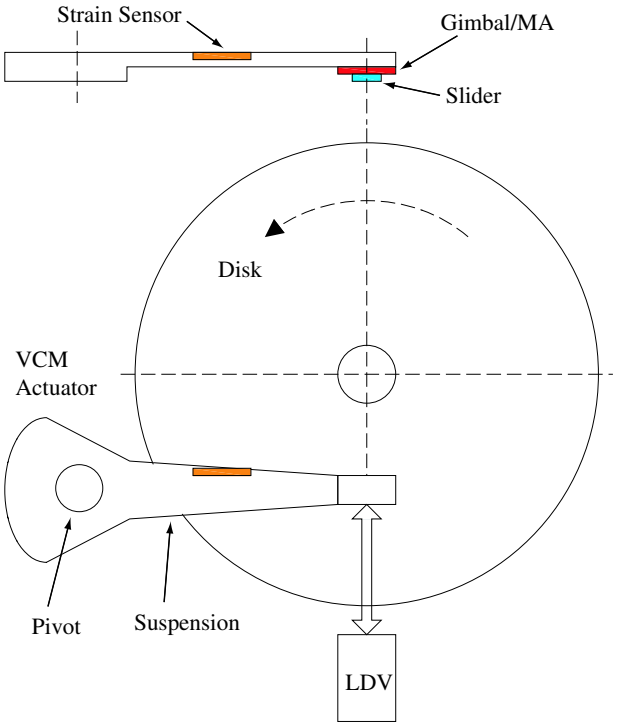

Figure 1: Dual-stage drive structure and suspension vibration measurement setup

Dual-stage servo systems can achieve a higher bandwidth than conventional single stage systems, and consequently further low frequency attenuation. However, the bandwidth of dual-stage servo is still limited by the PES sampling rage, which is limited by data storage efficiency. For example, the achievable bandwidth for a 40 kHz PES sampling rate is about 5 kHz. Since the excited vibration modes due to airflow have big components in the range of 6-12 kHz, this vibration cannot be efficiently attenuated by simply using PES feedback control even for dual-stage servo systems.

The hard disk structure is shown in Fig. 1. The lateral motion of the slider is measured with a laser doppler vibrometer (LDV) when the slider is flying on a 3.5-inch disk. The strain sensor is attached to the suspension at a proper location to sense the suspension vibration. This strain signal may be sensed at a faster sampling rate than that of the PES, and either active feedback damping control or feedforward compensation technique in addition to dual-stage servo to suppress the TMR due to airflow induced suspension vibration.

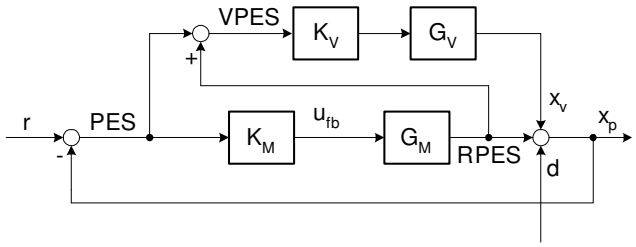

Figure 2: Block diagram of dual-stage control (DS)

The location and orientation of the sensor can be optimized to give the strongest correlation between the strain sensor output and the off-track motion of the slider due to suspension vibration. A method to search the optimal sensor location and orientation on the load beam has been proposed in [6], which maximizes the minimum singular value of the observability grammian of system's state space model.

3 Adaptive Vibration Compensation based on Dual-stage Servo

3.1 Dual-stage Servo Structure

The dual-stage servo structure, originally introduced by [7], is shown in Fig. 2. As shown in the figure, r represents the track runout, PES is the absolute tracking error of the head with respect to the data track center, while $RPES$ is the relative position error signal of the head relative to the tip of the suspension. The decoupling control approach utilizes the PES and $RPES$ to generate the position error of the suspension tip relative to the data track center, which will be labelled as $VPES$:

$$VPES = PES + RPES = r - x_v \,. \tag{1}$$

Due to this signal flow, it can be easily verified that the closed-loop sensitivity function from r to PES is the product of the VCM and MA loop sensitivity transfer functions, S_V and S_M:

$$S_T = S_V S_M \,, \tag{2}$$

where

$$S_V = \frac{1}{1 + K_V G_V}, \quad S_M = \frac{1}{1 + K_M G_M} \,, \tag{3}$$

where G_V and G_M are the TFs of the VCM and MA, respectively, and K_V and K_M are the loop compensators of the VCM and MA, respectively. Thus the dual-stage servo control design can be decoupled into two separate steps: the VCM loop, which is represented by S_V, and the MA loop, which is represented by S_M.

3.2 Adaptive Feedback and Feedforward Compensation of Suspension Vibration (MVC_FF)

The proposed adaptive vibration control structure is based on the above mentioned dual-stage servo control scheme. Its block diagram is shown in Fig. 3.

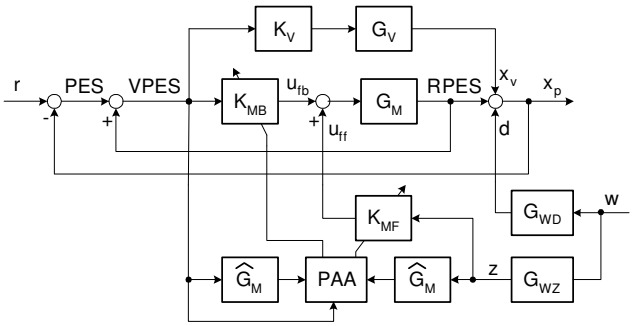

Figure 3: Block diagram of adaptive feedback plus feedforward control scheme (MVC_FF)

In this figure, w is the airflow excitation to the suspension, d is the head motion due to suspension vibration, G_{WD} is the TF from w to d, z is the strain sensor output, and G_{WZ} is the TF from w to z. Ideally, we would like z and d to have the highest degree of correlation. Since z and d represent vibrations at different locations of the suspension, d and z will reasonably be related by a dynamic relationship:

$$G_{ZD} = \frac{G_{WD}}{G_{WZ}} \,. \tag{4}$$

In this control structure, K_{MB} and K_{MF} are the feedback and feedforward compensators of the MA respectively. They are adapted in real time based on the minimum variance principle. The signal flow in this scheme is slightly different from that shown in Fig. 2. Here, the input to K_{MB} becomes $VPES$ rather than PES. This modification can be justified as follows. In the dual-stage scheme, the VCM loop is a stand-alone feedback controller, just like in the single stage case. The position error left by the VCM loop, $VPES$, can be taken as the disturbance to the MA, and the objective of the MA loop is to cancel this disturbance using feedforward control. The closed-loop TF from r to PES is

$$S_{rp} = \frac{1 - K_{MB}G_M}{1 + K_V G_V} \,, \tag{5}$$

and the TF from airflow disturbance w to PES is

$$S_{wp} = -\frac{(1 - K_{MB}G_M)G_{WD} + G_M K_{MF} G_{WZ}}{1 + K_V G_V} \,. \tag{6}$$

From Eq. (5), we can see that the ideal condition for runout compensation is $K_{MB}G_M \to 1$, then from Eq. (1), one obtains $PES \to 0$. Besides, for airflow induced disturbance attenuation, the feedforward controller, K_{MF}, should also be optimized. To achieve the best performance, the two compensators are updated online to minimize the variance of PES. To carry out the adaptation algorithm, the whole system is discretized with the sampling frequency of 40 kHz. All transfer functions and signals are expressed in the discrete time domain by using the sampling time index, k, and the unit delay operator, q^{-1}. Both K_{MB} and K_{MF} assume a finite impulse response (FIR) filter for stability considerations. They can be written as

$$\begin{aligned} K_{MB}(q^{-1}) &= K_{MB}(H_b; q^{-1}) \\ &= h_{b0} + h_{b1}q^{-1} + \cdots + h_{bn_B}q^{-n_B} \,, \end{aligned} \tag{7}$$

$$\begin{aligned} K_{MF}(q^{-1}) &= K_{MF}(H_f, q^{-1}) \\ &= h_{f0} + h_{f1}q^{-1} + \cdots + h_{fn_F}q^{-n_F} \,, \end{aligned} \tag{8}$$

where H_b and H_f are the filter parameter vectors $H_b = [h_{b0}\, h_{b1} \cdots h_{bn_B}]^{\mathrm{T}}$, $H_f = [h_{f0}\, h_{f1} \cdots h_{fn_F}]^{\mathrm{T}}$, and n_B and n_F are the orders of the FIR filters. In the following simulation, they are both taken to be 5.

For clarity, define $RPES$ as y_R, $VPES$ as y_V, and PES as y_P. Then the output of the MA becomes

$$\begin{aligned} y_R(k) &= G_M(q^{-1})(u_{fb}(k) + u_{ff}(k)) \\ &= G_M(q^{-1})(K_{MB}(q^{-1})y_V(k) + K_{MF}(q^{-1})z(k)) \\ &= K_{MB}(q^{-1})G_M(q^{-1})y_V(k) \\ &\quad + K_{MF}(q^{-1})G_M(q^{-1})z(k) \,. \end{aligned} \tag{9}$$

Let

$$x_b(k) = G_M(q^{-1})y_V(k) \,, \tag{10}$$

$$x_f(k) = G_M(q^{-1})z(k) \,, \tag{11}$$

and define the regressor vector

$$\begin{aligned} \phi(k) = [&x_b(k)\, x_b(k-1) \cdots x_b(k-n_B) \\ &x_f(k)\, x_f(k-1) \cdots x_f(k-n_F)]^{\mathrm{T}} \,, \end{aligned} \tag{12}$$

and the FIR tap weight vector

$$\theta = [h_{b0}\, h_{b1} \cdots h_{bn_M} h_{f0}\, h_{f1} \cdots h_{fn_F}]^{\mathrm{T}} \,. \tag{13}$$

Then the output equation of the MA can be written as

$$y_R(k) = \theta^{\mathrm{T}}\phi(k-1) \,. \tag{14}$$

Parameter adaptation algorithm (PAA) can be applied to estimate the coefficients of weight vector θ to minimize the mean squares value of MA tracking error, $e_M = y_V - y_R$, $E[|e_M(k)|^2]$. This is equivalent to minimizing the variance of PES, which gives the ultimate goal of the control system.

The regressor defined in Eqs. (10) and (11) will be estimated by passing y_V and z through the MA model, $\hat{G}_M$:

$$\hat{x}_b(k) = \hat{G}_M(q^{-1})y_V(k) \,, \tag{15}$$

$$\hat{x}_f(k) = \hat{G}_M(q^{-1})z(k) \,, \tag{16}$$

The estimation of $\hat{G}_M$ will be discussed in the next section.

The recursive least squares (RLS) PAA for tuning the tap weights of θ is [8]:

$$\hat{\theta}(k) = \hat{\theta}(k-1) + P(k)\phi(k-1)e(k) \,, \tag{17}$$

$$P(k+1) = \frac{1}{\lambda(k+1)}\left[P(k) - \frac{P(k)\phi(k)\phi^{\mathrm{T}}(k)P(k)}{\lambda(k+1) + \phi^{\mathrm{T}}(k)P(k)\phi(k)}\right] , \tag{18}$$

$$e(k) = y_R(k) - \theta^{\mathrm{T}}(k-1)\phi(k-1) \,. \tag{19}$$

The forgetting factor λ must satisfy $k\lambda(k) \to k$ as $k \to \infty$ in order for the controller parameter vector to converge. It should be properly chosen to obtain good convergence rate while ensuring stability. Other algorithms, such as the stochastic gradient approximation (SGA), also may be used.

3.3 MA Model Identification

The dynamics of a typical MEMS MA can be accurately described by a second order linear model without appreciable high order dynamics of up to 40 kHz [9]. However, due to lithographic misalignment and variations during etching processes, the resonance frequency of the MA, which has a nominal value of 1.5 kHz, may vary by as much as $\pm 15\%$ from its designed nominal value from one MA to another. Besides, the dynamics of a single drive are known to vary with age and use. These variations can be long term due to extended wear, or short term due to such factors as thermal effects, although time scales are typically long enough that the system can be modelled as time-invariant.

In the proposed adaptive control scheme, the MA model is needed to estimate the regressor states. With the measurement of $RPES$, the model can be estimated using extended recursive least squares method (ERLS). This PAA identifies the actual plant and noise model polynomials and obtains an estimate of the stochastic disturbance. The MA model can be described using a second order mass-spring-damper system model. The discrete time TF of the MA model can be written as

$$G_M(q^{-1}) = \frac{q^{-1}B_o(q^{-1})}{A_o(q^{-1})}\,, \tag{20}$$

where $B_o(q^{-1})$ and $A_o(q^{-1})$ are respectively the MA open-loop zero and pole polynomials:

$$B_o(q^{-1}) = b_0 + b_1 q^{-1}\,, \tag{21}$$

$$A_o(q^{-1}) = 1 + a_1 q^{-1} + a_2 q^{-2}\,. \tag{22}$$

Assume that $RPES$ is available, then the model parameter identification is based on the following model

$$A_o(q^{-1})y(k) = q^{-1}B_o(q^{-1})u_M(k) + w(k)\,, \tag{23}$$

where $u_M(k)$ is the actual input to the MA:

$$u_M(k) = u_{fb}(k) + u_{ff}(k)\,, \tag{24}$$

and $w(k)$ is the measurement noise of the $RPES$:

$$w(k) = C(q^{-1})n(k)\,, \tag{25}$$

and $n(k)$ is a white noise sequence. Based on this model, the extended least squares method can be applied to obtain $\hat{G}_M$.

3.4 Several Other Control Schemes Used for Comparison

To fully evaluate the performance of the proposed adaptive control scheme, several other control schemes are also simulated and compared with each other. They are briefly described as follows.

3.4.1 Dual-stage Control (DS)

The conventional dual-stage control scheme has been illustrated in Fig. 2. The compensators for VCM and MA, K_V and K_M, are fixed once designed. Airflow induced disturbance is still injected into the system but no feedforward compensation is added.

3.4.2 Minimum Variance Control (MVC)

The difference between this MVC scheme and the proposed adaptive control scheme is that in this MVC scheme, there is no feedforward signal. Only feedback compensator is adapted online based on minimum variance principle. It is expected that [10] this control scheme can yield better performance than pure feedback control scheme such as conventional dual-stage control.

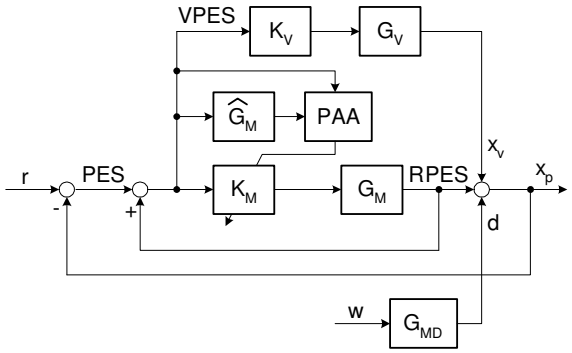

Figure 4: Block diagram of adaptive minimum variance control scheme (MVC)

3.4.3 Dual-stage plus Adaptive Feedforward Control (DS_FF)

The block diagram of dual-stage plus feedforward control scheme is illustrated in Fig. 5. In this scheme, the stain sensor signal is available for add-on adaptive feedforward control. Similar PAA as in the proposed scheme was applied in updating K_{MF}.

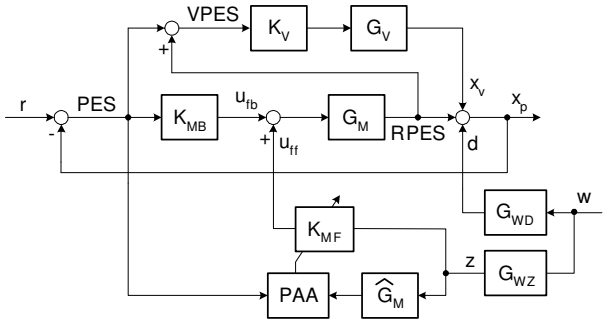

Figure 5: Block diagram of dual-stage plus feedforward control scheme (DS_FF)

4 Simulation Results

The sampling frequency used throughout the simulation is 40 kHz. The designed dual-stage feedback controller has an open-loop crossover frequency of 4.6 kHz. The runout, VCM and MA input disturbances, measurement noises of PES, $RPES$ and z are injected into the plant at corresponding locations.

4.1 Performance Comparison using RMS value

Table 1 shows the simulation results of those various types of control schemes. The control performance is indicated by the standard

Table 1: Performance comparison between several types of vibration control schemes

	MVC	DS	FF signal		Dstb	MA	MA	$\sigma(PES)$
			d	z	d	var	id	[nm]
1	◇			◇	◇	◇	◇	8.10
2	◇		◇		◇	◇	◇	6.91
3	◇		◇		◇	◇		85.70
4	◇			◇	◇			8.02
5	◇		◇		◇			6.72
6	◇		◇					6.05
7	◇				◇	◇		85.70
8	◇				◇			8.81
9	◇							6.03
10		◇	◇		◇	◇		11.43
11		◇		◇	◇			12.40
12		◇	◇		◇			9.16
13		◇	◇					6.72
14		◇			◇	◇		17.30
15		◇			◇			15.85
16		◇						6.70

deviation of PES, which is donated as $\sigma(PES)$. The meaning for each column is as follows. MVC means that K_{MB} is adapted using minimum variance principle. DS is dual-stage control scheme with fixed compensator gains. FF signal shows which signal, d or z, is used as the measured signal in feedforward control. If neither of them is checked, then there is no feedforward control. Dstb is the airflow induced vibration disturbance to suspension. MA VAR means there is MA model variation. In the simulation, the natural frequency ω_M changes 15% from its nominal value. MA ID is the MA model identification function.

From this table, the following remarks can be concluded.

1) *Performance comparison between nominal systems*. Comparing the results of (5) (8) (12) and (15), we can see that the reduction of $\sigma(PES)$ from DS to MVC and DS_FF is about 43%, while from DS to MVC_FF is about 58%. MVC_FF has the best nominal performance. This comparison shows that adaptation mechanism can effectively compensate for airflow induced suspension vibration.

2) *The impact of suspension vibration on system performance.* It is noted that without actual disturbance, the adaptation mechanism still runs using the virtual measurement of z. Comparing (5) with (6), (8) with (9), (12) with (13), and (15) with (16), we can see that the MVC_FF has the smallest degradation due to d, of only about 9%, while the DS deteriorates at about 137%. MVC and DS_FF deteriorate at about 46% and 36%, respectively. This is consistent with the comparison results from nominal systems.

3) *Difference between direct measurement d and indirect measurement z for feedforward control.* As is expected, the performance of the direct measurement cases, (5) and (12), is better than that of the indirect measurement cases, (4) and (11). The deterioration from (5) to (4) is smaller than that from (12) to (11). Therefore, it can be concluded that MVC_FF is not so sensitive to measurement signal quality than DS_FF.

4) *Effect of deviations between actual and nominal MA plants*. This is to investigate the sensitivity of the adaptive control to the MA model variation. The MA model is needed in DS_FF, MVC and MVC_FF. From (3) and (7), it can be seen that, without additional MA model identification, both MVC and MVC_FF are extremely sensitive to MA model variation. Therefore, for MVC and MVC_FF to work effectively, MA model identification loop should be incorporated into the systems.

5) *Effect of MA plant identification*. This comparison is to check how much of the performance can be recovered from the degradation due to MA model variation. With MA identification, the MVC_FF system (2) recovers most of its performance as in the nominal case (5).

4.2 Frequency and time domain responses

To fully explore system performance of various types of control schemes, analyses of frequency and time domain responses are carried out.

Figs. 6-9 show the normalized spectra of the four types of control schemes. Their standard deviations are already shown in Table 1. From Fig. 6, we can see that track runout and low frequency disturbances have been greatly attenuated by the high bandwidth feedback controller. However, there are peaks in the range of 6-12 kHz, which are due to airflow excited suspension vibrations. From Figs. 7-9, we can see that both MVC and FF controls can effectively suppress the airflow induced suspension modes. The minimum variance feedback control attenuates disturbances in the low frequency range, while the adaptive feedforward control attenuates disturbances in the high frequency range. In Fig. 8, the waterbed effect can be observed, i.e., high frequency vibrations are amplified a little bit by MVC feedback control. The MVC_FF has the best disturbance attenuation in both low and high frequency ranges.

Figs. 10-12 show the evolutions of feedback and feedforward FIR coefficients, H_b and H_f, and MA model parameters, H_m, for MVC_FF control with MA plant variation and MA model identification. As can be seen, the adaptation processes of H_b and H_f take place after H_m roughly converges to its true values. Therefore, the whole adaptation process takes a little longer time, which is about 0.1 s. While from Fig. 13, it shows that the time response of PES converges since the time point of about 0.05 s, even though during the period of 0.05-0.1 s, the FIR parameters, especially that of K_f, still change greatly. This phenomenon will be investigated in detail in the future research.

The convergence problem can be alleviated in the following two ways. First, since the sampling rates of PES and vibration signal are not limited by data storage efficiency, which limits the sampling rate of PES, the MA model identification can be run at a higher rate. This will reduce the settling time of MA identification and in turn shorten the overall settling time. Furthermore, the adaptive feedforward control loop can be run at a higher rate, it is expected that further attenuation of high frequency suspension vibration can be achieved due to wider dynamic bandwidth. Second, an algorithm similar to the one developed in [2] by incorporating an additional plant and nose model identification PAA. It is expected that that algorithm will result in a faster convergence rate. Alternatively, we can use an off-line pre-tuning process to establish a table of the optimal feedforward filter coefficients with respect to different locations on the disk. The feedforward filter can then be fine tuned in real time.

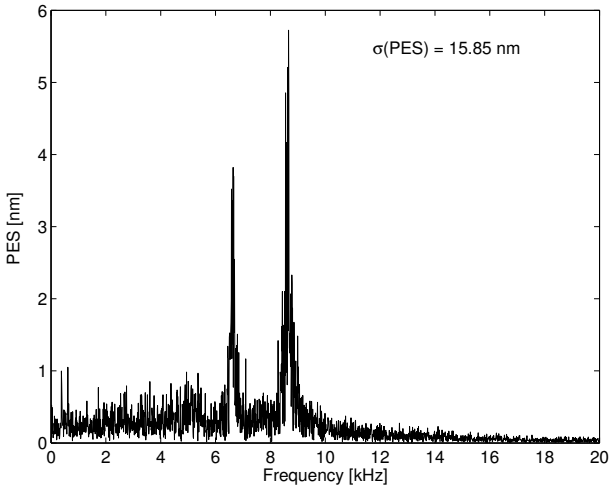

Figure 6: Spectrum of PES for DS control

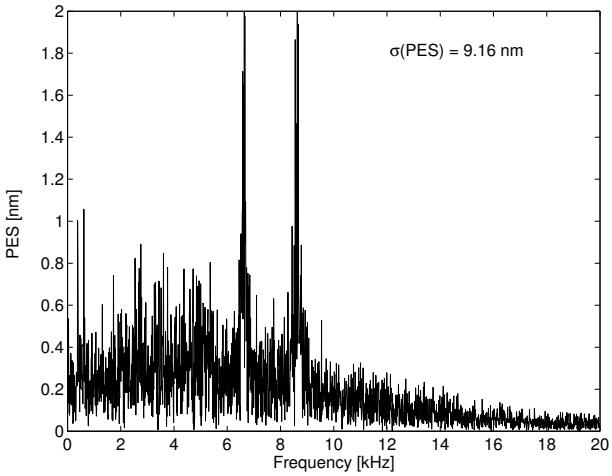

Figure 7: Spectrum of PES for DS_FF control

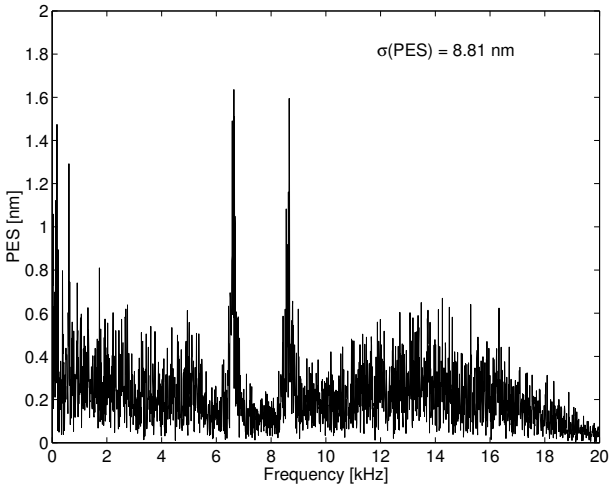

Figure 8: Spectrum of PES for MVC control

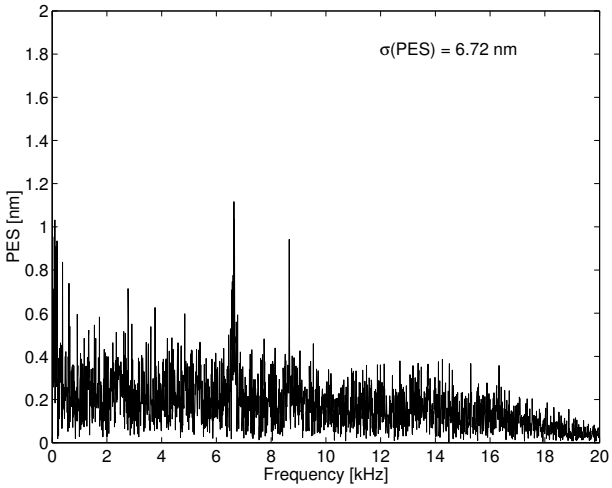

Figure 9: Spectrum of PES for MVC_FF control

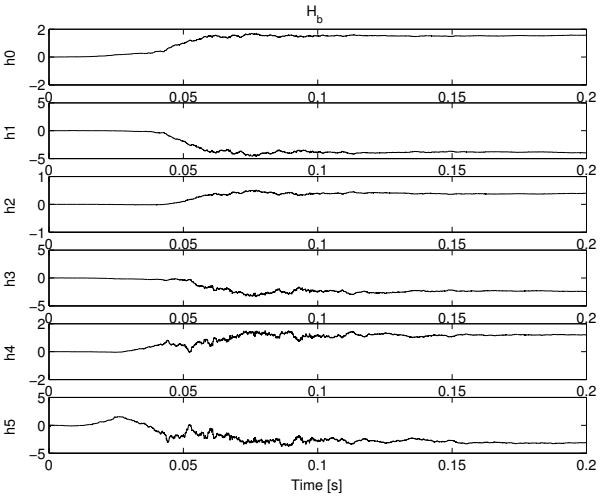

Figure 10: Feedback FIR adaptation for MVC_FF control with MA plant variation and model identification

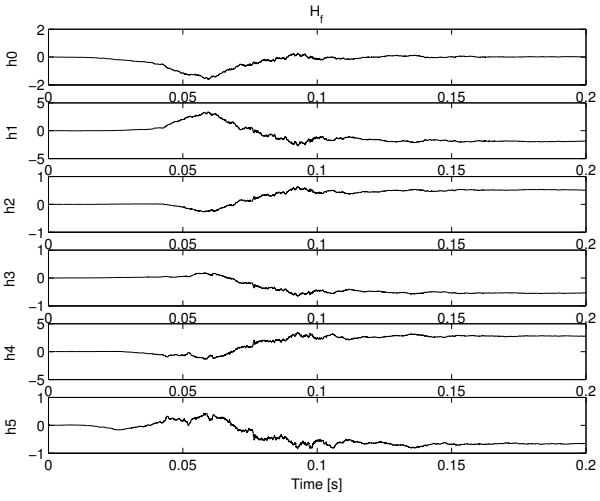

Figure 11: Feedforward FIR adaptation for MVC_FF control with MA plant variation and model identification

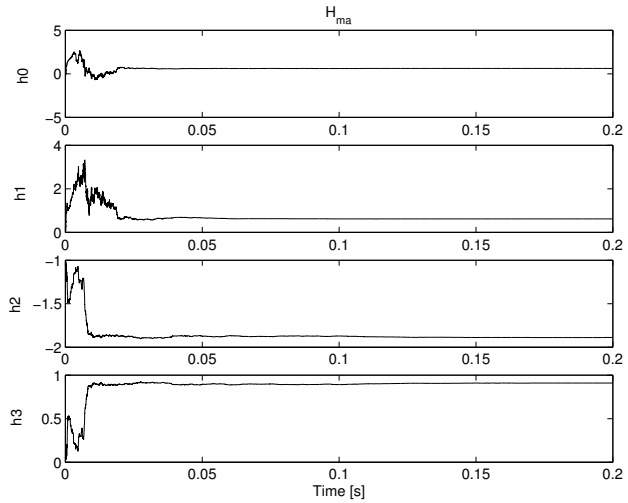

Figure 12: MA model parameters adaptation for MVC_FF control with MA plant variation and model identification

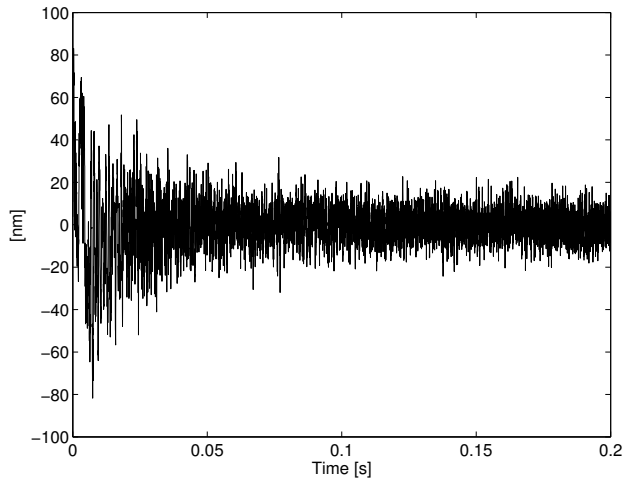

Figure 13: Time response of PES for MVC_FF control with MA plant variation and model identification

5 Conclusions

Airflow induced suspension vibration poses a significant challenge to the next generation of high density, high RPM and high performance hard disk drives. By incorporating additional vibration sensors into instrumented suspension and using adaptive control scheme, suspension vibration can be greatly attenuated with dual-stage actuators. In this paper, an adaptive feedback and feedforward control scheme was developed. Its performance was explored based on the comparison with several other control schemes and from the frequency and time domain responses. Robustness and convergence problems are considered. It is expected that this new adaptive control scheme will yield excellent performance when the robustness and convergence problems are properly handled.

Future work related to this paper includes, design and fabrication of vibration sensors using piezo-electronics, development of multi-rate control scheme with adaptation and identification loops running at a faster rate than the feedback loop, and experimental validation of the proposed vibration compensation scheme.

References

[1] C. Mohtadi and M. A. Dphil, "Bode's integral theorem for discrete-time systems," *IEE Proceedings D*, vol. 137, March 1999.

[2] S. Pannu and R. Horowitz, "Increased disturbance rejection for hard disk drives using accelerometers," *The Journal of Information Storage and Processing Systems*, vol. 1, pp. 95–103, 1999.

[3] S.-E. Baek and S.-H. Lee, "Vibration rejection control for disk drives by acceleration feedforward control," in *Proceedings of the 38th Conference on Decision and Control*, Phoenix, Arizona, December 1999.

[4] R. Oboe, "Use of low-cost mems accelerometers for vibration compensation in hard disk drives," in *Proceedings of the 6th International Workshop on Advanced Motion Control*, 2000.

[5] Y. Li and R. Horowitz, "Active suspension vibration control with dual-stage actuators in hard disk drives," in *Proceedings of American Control Conference*, vol. 4, 2001, pp. 2786–2791.

[6] Y. Huang, M. Banther, P. D. Mathur, and W. Messner, "Design and analysis of a high bandwidth disk drive servo system using an instrumeted suspension," *IEEE/ASME Transaction of Mechatronics*, vol. 4, no. 2, pp. 196–206, 1999.

[7] K. Mori, T. Munemoto, H. Otsuki, Y. Yamaguchi, and K. Akagi, "A dual-stage magnetic disk drive actuator using a piezoelectric device for a high track density," *IEEE Transactions on Magnetics*, vol. 27, pp. 5298–5300, Nov. 1991.

[8] K. J. Åström and T. Hägglund, *PID Controllers, Theory, Design and Tuning*, 2nd ed. Instrument Society of America, 1995.

[9] L.-S. F. *et al*., "Electorstatic microactuator and design considerations for hdd application," *IEEE Transactions on magnetics*, vol. 35, no. 2, March 1999.

[10] R. Horowitz and B. Li, "Adaptive track-following servos for disk file actuators," *IEEE Transactions on Magnetics*, vol. 32, no. 3, pp. 1779–1786, 1996.